International Journal of Core Engineering & Management
Volume-6, Issue-12, 2021 ISSN No: 2348-9510

THERMO-FATIGUE-AWARE LATTICE OPTIMIZATION FOR LIGHTWEIGHT ADDITIVELY MANUFACTURED ROTATING COMPONENTS

Rupesh Rameshrao Dhore
Catia Designer
Altair Product Design Inc.
Canton, MI, USA
rupeshdhorey@gmail.com

Abstract

Impellers, compressor wheels and turbine discs are examples of rotating parts that are too lightweight for traditional manufacturing methods and are good candidates for lattice infill produced with LPBF, but their design is limited by the interplay of centrifugal loading, thermal history and the high susceptibility of additively manufactured metals to fatigue. Twenty-two studies ranging from process physics to defect characterization, microstructural anisotropy, fatigue of bulk and cellular materials, residual stress and structural optimization were reviewed in this systematic review to formulate a framework for lattice optimization considering thermo-fatigue. First, the literature was reviewed to identify four themes, and quantitative data were converted to a common unit. Then, the governing relations were synthesized into a single design formulation that minimizes mass while complying with centrifugal and thermal equilibrium constraints, the defect-based Goodman fatigue criterion summed by a norm-based measure, and design for additive manufacturing constraints. The synthesis indicates that by careful design of a build, relative densities of near 99.8 percent can be achieved in the aluminum alloy; with careful machining and HIP processing, fatigue strengths of approximately 200 to 300 megapascals should be obtained as-built; and lattice fatigue strengths should be in the range of 0.1 to 0.3 times the static yield strength of the material. The final design features cells dominated by stretches, smooth minimal surfaces and cells with radial density grading as a function of the hoop stress distribution, and stress relief requirements. However, there are still some limitations in stress constrained optimization, including the immaturity of the stress constrained optimization, lack of access to the inner surface of the lattice, and absence of fatigue data at higher temperatures for superalloy lattices.

Index Terms—Additive manufacturing, lattice structures, topology optimization, fatigue, residual stress, rotating components, laser powder bed fusion, lightweight design, thermo-mechanical analysis

I. INTRODUCTION

In elements, such as impellers, and compressor and turbine wheels and fans, centrifugal vibration thermal, loading occur concomitantly so mass, and thus the moment of inertia the

bearing loads the energy used are significant. Laser sintering (selective laser sintering (SLS) also referred to as laser powder bed fusion (L-PBF)) provides the ability to create internal cell architectures that cannot be created by the casting or machining process in order to reduce material use for less onerous load paths. AlSi10Mg alloys are also relatively light (density of about 2.67 g/cm3) and are preferred for the use at low temperatures for rotors, but these alloys are not processable because of porosity. When the relative density is coordinated with the scanning speed, the hatch spacing and a two-pass scanning strategy, the process window can be used to control the relative density, which has been shown to approach 99.8% for thin load-bearing features [1].

Hot-section rotating components have to meet more severe constraints as they demand high creep and endurance strength from the nickel-base super alloy at elevated temperature levels. Alloys that have a higher γ′ content, such as the highly γ' strengthened alloys (e.g., CM247LC), are likely to suffer from strain-age cracking and solidification cracking during L-PBF processing. The presence of columnar microstructures, residual stresses and the often-required hot isostatic pressing (HIP) make qualification more complex and to date have limited the use of lattice-filled superalloy rotors to research demonstrators and not to certified hardware [2].

Fatigue, not static strength is the basis for design of rotating parts in all alloy classes; each time the rotation shut off, it is known as a low cycle load reversal, but each time the blades pass, and each time the imbalance excitation, it is known as a high cycle load reversal. The disadvantages of metals produced by additive manufacturing processes are much more highly influenced by defect size than those of wrought metals: lack-of-fusion pores, gas pores and surface notches are all pre-existing cracks and the fatigue limit is determined by the largest defect, not its matrix structure. Fatigue strengths of additively manufactured and conventional materials can be plotted on the same basis on the common Kitagawa-Takahashi diagram which provides quantitative correlation between inspection data and design allowables [3]. These observations are then merged in a thermo-fatigue-informed framework of lattice optimization in the following review.

II. REVIEW METHODOLOGY AND ANALYTICAL FRAMEWORK

This systematic review protocol was used to search 22 peer-reviewed sources between 2013 and 2020 in journals from the areas of additive manufacturing, fatigue, structural optimization and computational mechanics. Sources were selected according to the relevance to the selected themes: process physics, defect and microstructure effects, fatigue of bulk and cellular materials, and optimization methodology; quantitative data were taken out of the sources and interpreted in SI-units. A process–structure–property relationship, which had been developed for metallic AM, where the phase constitution is determined by the cooling rates between 103 and 106 K/s, followed and was used as an organizing taxonomy for [4]. The themes that were drawn from the literature are summarized in table 1 and the screening and synthesis process is summarized in fig. 1.

International Journal of Core Engineering & Management
Volume-6, Issue-12, 2021 ISSN No: 2348-9510

Table 1: Mapping of Reviewed Literature to the Thematic Framework

Theme	References	Principal contribution to the framework
Process physics and thermal history	[4], [7], [14], [20]	Thermal cycles, cooling rates, residual stress formation and measurement
Porosity and defect characterization	[1], [6], [12]	Process windows, CT-based defect statistics, geometric imperfections of struts
Microstructure and anisotropy	[2], [8]	Columnar grains, cracking of superalloys, orientation dependence of properties
Fatigue of bulk alloys	[3], [9], [19]	Defect sensitivity, √area approach, effect of post-processing
Fatigue of lattices	[10], [22]	Load-mode and unit-cell effects on normalized S–N behavior
Lattice design and modeling	[5], [13], [17], [21]	Homogenization, unit-cell selection, density grading, lightweight steel lattices
Optimization methodology	[11], [15], [16], [18]	SIMP and level-set methods, AM constraints, DfAM rules, infill optimization

Note. Themes correspond to the screening categories shown in Fig. 1.

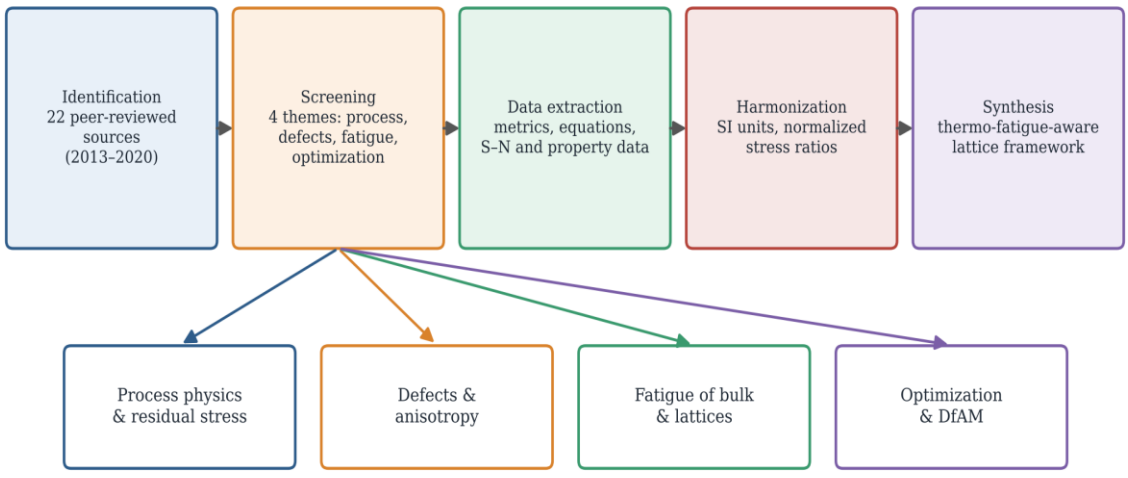


Figure 1: Systematic Review Workflow and Thematic Classification of the Reviewed Sources

International Journal of Core Engineering & Management
Volume-6, Issue-12, 2021 ISSN No: 2348-9510

III. LATTICE ARCHITECTURES AND HOMOGENIZED MODELING

Periodic or graded structures with effective properties defined by the topology of the unit-cell and relative density, which are composed of struts, sheets or shells. For the additively manufactured lattices, different modeling methods were employed, from analytical beam-theory solutions to complete finite element models with beam or solid elements, with increasingly more cells being used (up to thousands) and the accuracy versus cost being taken into consideration. Generally, the behaviour of the effective stiffness is shown to be a power law of the relative density as shown in Eq. 1 with n equal to 2 for bending-dominated cells and to 1 for stretching-dominated cells and C a geometric constant. The Maxwell number, in the second equality of Eq. 2, with b number of struts, j number of joints, and M ≥ 0 stretching dominance [5] defines the topology.

$$\frac{E^*}{E_s} = C\left(\frac{\rho^*}{\rho_s}\right)^n \quad (1)$$

$$M = b - 3j + 6 \quad (2)$$

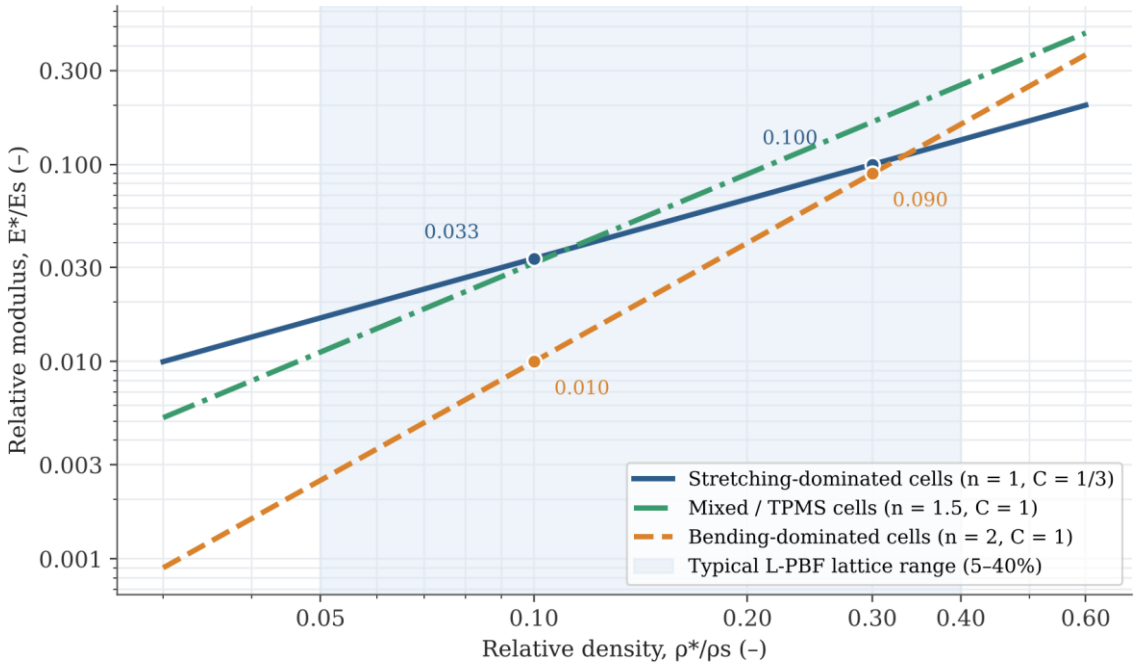


Figure 2: Relative Modulus Versus Relative Density for Stretching-, Mixed- and Bending-Dominated Lattices According to Eq. 1

International Journal of Core Engineering & Management
Volume-6, Issue-12, 2021 ISSN No: 2348-9510

IV. PROCESS-INDUCED DEFECTS, MICROSTRUCTURE AND ANISOTROPY

A. Defect Populations and Process Parameters

The study of defects that govern fatigue in AM parts has been the focal point of interest for quantifying using X-ray computed tomography (CT) technique. Tomographic studies have shown that irregular lack-of-fusion voids, spherical gas pores, keyhole pores caused by too high energy input, and near-surface pores at contour-hatch boundaries are common defects.In well-optimized parts, porosity is usually very low, less than 0.5%, but the size, shape, and placement of the largest pores can have a bigger impact on fatigue performance.Another type of defect is surface roughness, which forms from the partial fusion of powder particles, especially on the bottom surface of thin struts.These areas cannot be machined after printing, and the defects here are especially harmful to the fatigue strength of thin struts.

The volumetric energy density, as shown in equation 3, connects the number and type of defects with the processing parameters.The way processing affects the number of defects is through the volumetric energy density described in equation 3. If the energy is too low, there will be no fusion porosity, if it is too high there will be keyhole pores and volatilization of elements. Rapid solidification, as mentioned above, implies that the as-built alloys have very fine microstructures with ultimate tensile strengths similar or higher than those of the cast and wrought ones, as shown in Table 2, and in many cases the elongation is less than 10% [7] for the as-built Ti-6Al-4V with the martensitic α′ microstructure. A comparison of typical strengths of the major rotor alloys is given in Figure 3.

$$E_v = \frac{P}{vht} \qquad (3)$$

Table 2: Representative L-PBF Material Data for Rotating-Component Alloys

Alloy	Density (g/cm³)	Typical rotating application	As-built UTS (MPa)	As-built elongation (%)	Principal processing concern
AlSi10Mg	2.67	Impellers, fan hubs (below about 150 °C)	350–460	3–8	Gas porosity, oxide films
316L	7.9	Pump impellers, corrosion-resistant rotors	550–700	15–45	Residual stress, lack of fusion
Ti-6Al-4V	4.43	Compressor blisks, fan rotors (below about 400 °C)	1,100–1,300	4–10	Brittle α′ martensite, residual stress
Inconel 718	8.19	Turbine discs, shafts (below about 650 °C)	1,000–1,200	15–30	Segregation, Laves phase, anisotropy

Note. UTS = ultimate tensile strength. Ranges are representative of values reported in the reviewed literature for as-built, horizontally oriented specimens.

International Journal of Core Engineering & Management
Volume-6, Issue-12, 2021 ISSN No: 2348-9510



Figure 3: Ultimate Tensile Strength of As-Built L-PBF Rotor Alloys Compared with Conventional References

B. Microstructural Anisotropy

The columnar grains are found to span several layers when growing epitaxially in Ti-6Al-4V prior-β grains and in nickel alloys columnar γ grains are not uncommon. The way crystals are arranged and their shapes affect how they respond to stress, leading to differences in how stiff they are, how stretchy they are, and how well they resist getting tired from repeated use.The most important direction for stress to cause problems in gaps from poor fusion is when the stress is applied straight up and down through the layers or along the direction the part was built.Another kind of difference comes from how the part was heated and cooled, especially in parts with very thin struts and solid centers.So, when designing parts that spin, it's important to think about how the struts are placed compared to the spinning axis and the forces they experience.

V. FATIGUE PERFORMANCE OF BULK AND LATTICE MATERIALS

Looking at the fatigue data from making Ti-6Al-4V with additive manufacturing, the main factors that affect how long the material can last under repeated stress were surface roughness, holes in the material, and the structure of the material. Surface roughness had the biggest effect on how well the material could stand up to fatigue.The strength of parts made directly without extra processing was about 200 to 300 MPa after 10^7 cycles, but after some extra steps like

International Journal of Core Engineering & Management
Volume-6, Issue-12, 2021 ISSN No: 2348-9510

machining and heat treatment, the strength got closer to that of metal made using traditional methods, reaching 500 to 600 MPa, as shown in Table 3.

The Murakami formula, given in equation 4, helps estimate how well the material can handle small flaws; it uses the fatigue limit in MPa, the hardness of the material, the size of the flaw in square micrometers, and a coefficient that depends on whether the flaw is on the surface or inside the material. The Basquin formula, given in equation 5, describes how the material behaves under repeated stress over a limited number of cycles, using stress amplitude, a strength factor, the number of cycles to failure, and an exponent that describes how the strength changes with the number of cycles.

$$\sigma_w = \frac{C(HV+120)}{(\sqrt{area})^{\frac{1}{6}}} \quad (4)$$

$$\sigma_a = \sigma_f'(2N_f)^b \quad (5)$$

Table 3: Influence of Post-Processing on the Fatigue Strength of L-PBF Ti-6Al-4V

Condition	Dominant crack initiator	Fatigue strength at 10^7 cycles (MPa)	Ratio to wrought (%)
As-built surface	Surface roughness, near-surface pores	200–300	35–55
Machined, stress relieved	Internal lack-of-fusion pores	350–450	65–80
HIP, as-built surface	Surface roughness	250–350	45–65
HIP and machined	Microstructural features (α colonies)	500–600	90–110
Wrought reference	Microstructure	approximately 550	100

Note. Ratios are computed against a wrought reference of approximately 550 MPa.

Fatigue in lattices is different from in solid materials because the points where the struts meet act as stress points and the surfaces of the struts can't be smoothed out easily. Testing showed that the lifespan of Ti-6Al-4V lattices was very sensitive to how much the load was applied and the type of load.The longest lifespan was seen when the load was purely compressive, but loads that included tension shortened the lifespan because cracks started at the points where the struts meet under tension.The strength after 10^6 cycles was about 0.1 to 0.3 of the yield strength, which is much less than that of traditionally made metals. Because of the mostly tensile stresses caused by spinning and the vibrations involved, the data showing how the material behaves under tension is used when designing the parts that connect the spinning components, as shown in the example curves in Figure 4.

International Journal of Core Engineering & Management
Volume-6, Issue-12, 2021 ISSN No: 2348-9510

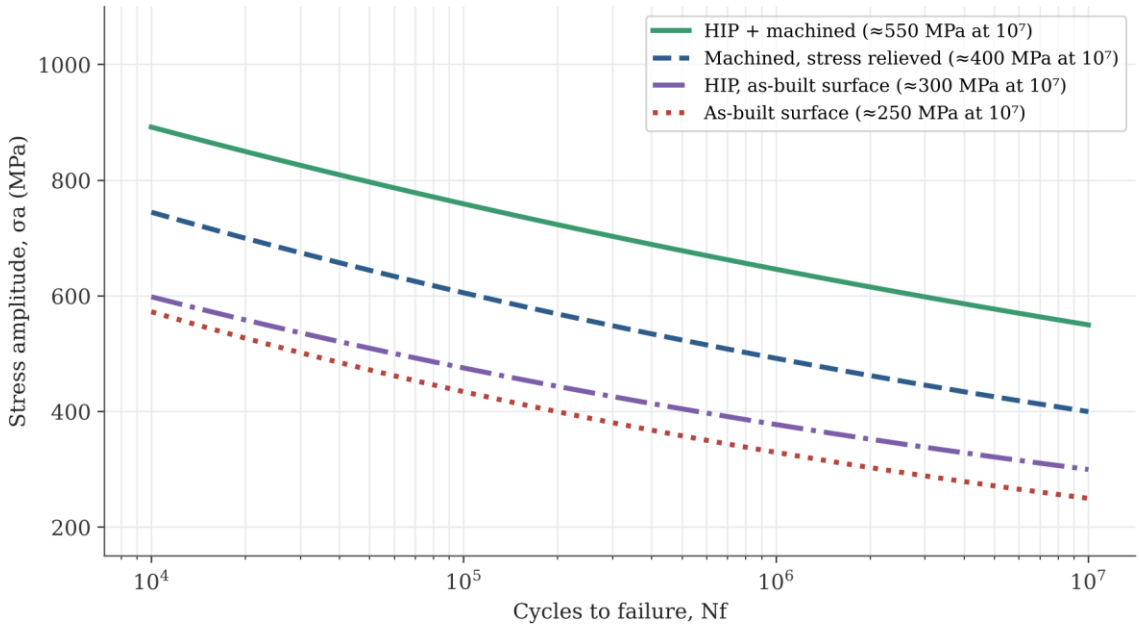


Figure 4: Representative Basquin S–N Curves for L-PBF Ti-6Al-4V in Different Post-Processing Conditions

VI. OPTIMIZATION FRAMEWORKS FOR LATTICE DESIGN

Topology optimization (TO) for AM has progressed from stiffness optimization to formulations that include manufacturing constraints, multi-scale lattice representations and multiphysics responses. The solid isotropic material with penalization (SIMP) approach summarized in the above equation (6) interpolates between the void modulus Emin and solid modulus E0 with the density variable ρe and penalization exponent p, which is normally assigned a value of 3. Overhang angle constraints that lead to elimination of support structures, length-scale control to allow minimum printable features, and concurrent macro–micro schemes, in which the lattice properties are homogenized instead of solid material is used in the intermediate-density regions, have been reported. The stress and fatigue based variants did not progress as far as the compliance based variants as the stress and singularity phenomena are local at low densities.

$$E(\rho_e) = E_{\min} + \rho_e{}^p (E_0 - E_{\min}) \qquad (6)$$

The assumption for the ideal lattice geometry leads to the systematic over prediction of the lattice performance since L-PBF introduces a lattice strut diameter variation and introduces some waviness in the struts and an oversized surface in the bottom surfaces of the lattices. It was found that when reconstructing the imperfect metallic lattices using micro-CT, combined

with finite element analysis, the geometric defects decreased the elastic stiffness and initial failure strength of the lattice compared to the lattice as designed, and also influenced the failure sequence by localizing strain into the thinnest struts [12]. Therefore it is important that a defect-aware formulation should employ the homogenized properties, or sample the diameters of the computer-aided design parts from the measured diameter distribution, not from the nominal distribution.

Also, bounds on manufacturable designs have been laid out in the SLM lattice literature. Typical diameters of the struts vary between 0.2 and 1.0 mm, unit cells between 2 and 10 mm and relative density between 5 and 40%.Common diameters of the struts are in the range of 0.2-1.0 mm, and the size of the unit cell is typically in the range of 2-10 mm, with the relative density typically in the range of 5-40%.

The body-centred and face-centred varieties are good for stiffness in terms of elongation, whereas the triply periodic minimal surfaces (TPMS), such as gyroids, are good for smooth geometries which support themselves with low stress concentration, and are often strutted vertically, making them more printable. Table 4 is a comparison of the candidate unit cells with the criteria that are appropriate for rotating components.

Table 4: Comparison of Candidate Unit Cells for Rotating Lattice Components

Unit cell	Deformation mode	Maxwell number	Stiffness exponent n	Self-supporting	Fatigue-relevant feature
Body-centered cubic (BCC)	Bending	$M < 0$	≈ 2	Yes (struts at 35.3°)	Sharp nodes, low normalized endurance
BCC with vertical struts	Mixed	$M < 0$	1.5–2	Yes	Higher axial stiffness, node stress concentration
Octet truss	Stretching	$M \geq 0$	≈ 1	Partly (horizontal struts)	High stiffness per mass
Diamond	Bending	$M < 0$	≈ 2	Yes	Uniform strut lengths, moderate endurance
Gyroid (TPMS)	Mixed	Not applicable	1.5–2	Yes	Smooth curvature, lower stress concentration
Simple cubic	Stretching (axial)	$M = 0$	≈ 1 (axial)	No (horizontal struts)	Weak in shear, orientation sensitive

Note. Maxwell number from Eq. 2; exponent n from Eq. 1.

International Journal of Core Engineering & Management
Volume-6, Issue-12, 2021 ISSN No: 2348-9510

VII. THERMAL HISTORY AND RESIDUAL STRESS

The large temperature differences and restriction of contraction during the deposition of the different layers of material cause residual stresses which can attain the strength-limit of the alloy under deposition. A model that integrates heat transfer and fluid flow with thermo-mechanical analysis made it possible to better predict residual stress and distortion, while a dimensionless strain parameter indicated that the thermal strain increases with increasing heat input and decreasing thermal diffusivity of the alloy [14]. The approximation of the stress caused by a confined thermal change ΔT is given by Eq.7, where E is Young's modulus, α is the coefficient of thermal expansion and ν is Poisson's ratio. Residual stress is taken into account in the modified Goodman relation (Eq. 8) as a mean stress in addition to the service loading and therefore is a mean stress on top of the service loading.

$$\sigma_{\text{th}} = \frac{E\alpha\Delta T}{1-\nu} \tag{7}$$

$$\frac{\sigma_a}{\sigma_w} + \frac{\sigma_m + \sigma_{\text{res}}}{\sigma_u} \leq \frac{1}{S_f} \tag{8}$$

Table 5: Thermophysical Properties Governing Residual Stress in Rotor Alloys

Alloy	E (GPa)	α (10^{-6}/K)	k (W/m·K)	Diffusivity (mm^2/s)	Eα/(1−ν) (MPa/K)	Gradient tendency
AlSi10Mg	70	21.0	130	≈ 54	2.19	Low
316L	193	16.0	16.2	≈ 4.1	4.41	Moderate
Ti-6Al-4V	114	8.6	6.7	≈ 2.9	1.49	High
Inconel 718	200	13.0	11.4	≈ 3.2	3.66	High

Note. The stress index Eα/(1−ν) follows Eq. 7 per kelvin of constrained temperature change; low diffusivity increases the temperature gradients to which the index is applied.

VIII. THERMO-FATIGUE-AWARE OPTIMIZATION FORMULATION

A. Problem Statement

The most structured approaches are density-based, level-set, topological-derivative, phase-field and evolutionary TO which share a common structure: design parametrization, finite element state equation, sensitivity analysis, mathematical programming update, and density-based schemes with filtering are the most robust methods for large three-dimensional problems [15]. On top of this, a thermo-fatigue-aware formulation is generated as Eq. 9, in which mass is to be minimised over the set of lattice relative densities that satisfy the equilibrium under the centrifugal loading fω and thermal loading fT, a fatigue constraint and the density bounds. With the defect adjusted fatigue limits given in Eq. 4, ηe (Eq. 8) are computed for each element

International Journal of Core Engineering & Management
Volume-6, Issue-12, 2021 ISSN No: 2348-9510

Goodman and aggregated using the P-norm measure given in Eq. 10. The load is not a typical compliance load, but rather it is dependent on the design, since it's proportional to ω2 and the local density.

$$\begin{aligned} &\min_{\rho} \; m(\rho) = \sum_{e=1}^{N_e} \rho_e \rho_m V_e \\ &\text{subject to } K(\rho)u = f_\omega(\rho) + f_T(\rho) \\ &\eta_{PN}(\rho) \le 1, \quad \rho_{\min} \le \rho_e \le 1 \end{aligned} \tag{9}$$

$$\eta_{PN} = \left(\sum_{e=1}^{N_e} \eta_e^{\,P}\right)^{\frac{1}{P}} \tag{10}$$

B. Manufacturing Constraints

In the optimization result always there are rules that have to be followed in the design process: Design for Additive Manufacturing (DfAM) that are based on the process limitation. Published guidelines suggest that the angle of the overhangs must not exceed 45° and that the minimum wall thickness should be based on the width of the melt pool, in addition to the need for powder removal paths for enclosed cells, and that the effect of build orientation on surface quality and accuracy should be taken into account. These considerations also have cost implications as the removal of support, post processing and inspection might be much more significant when manufacturing small batch aerospace hardware [16]. They are enforced in the synthesized framework by applying overhang filters to the input signals, minimum-density bounds to the output signals, and orientation-dependent knockdown factors which form the iterative loop that is depicted in Fig. 5.

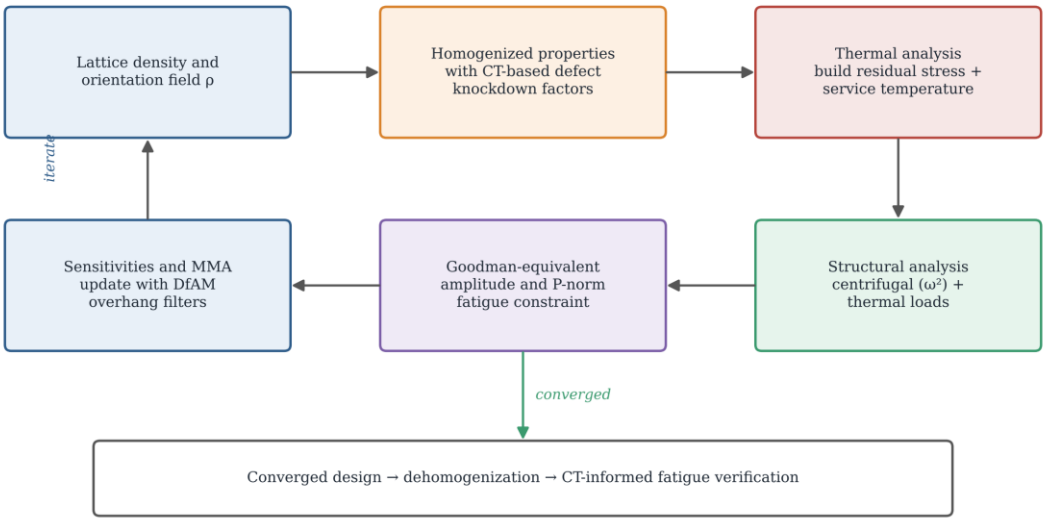


Figure 5: Iterative Thermo-Fatigue-Aware Lattice Optimization Loop

International Journal of Core Engineering & Management
Volume-6, Issue-12, 2021 ISSN No: 2348-9510

C. Density Grading and Infill

Spatially graded lattices are especially suitable for rotors because stresses decrease from the bore to the rim which can be predicted by elasticity. The hoop stress in a solid disc of radius R with an angular velocity ω is given by Eq. 11, with ρm denoting the material density and r the radial coordinate. One such approach for design of graded lattices with optimized mesostructures was developed where the cell density was optimized to the local stress field, resulting in stiffer lattices with connections between neighbouring cells vs uniform lattices of equal mass [17]. This is illustrated in Fig. 6 where the analytical stress distribution and implied density grading for a solid Ti-6Al-4V disc of 150 mm radius rotating at 20,000 rpm is presented, and it is seen that the hoop stress decreases from ~183 MPa at the centre to ~72 MPa at the rim of the disc, while the disc mass is removed at the rim, centrifugal load decreases at the bore.

$$\sigma_\theta = \frac{3+\nu}{8}\rho_m \omega^2 R^2 \left[1 - \frac{1+3\nu}{3+\nu}\left(\frac{r}{R}\right)^2\right] \quad (11)$$

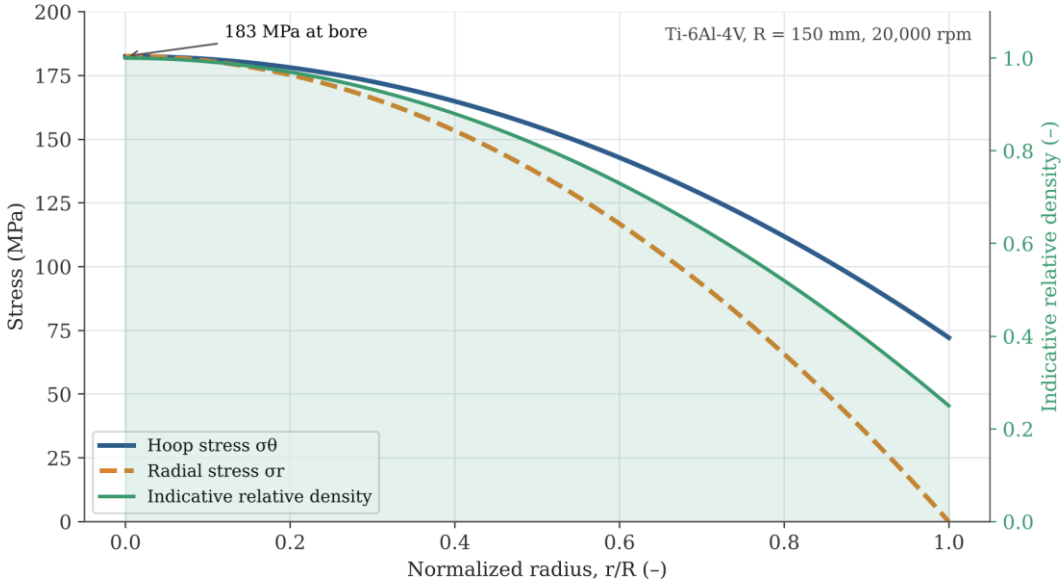


Figure 6: Hoop and Radial Stress Distributions in a Rotating Solid Ti-6Al-4V Disc with Indicative Radial Density Grading

Other explicit unit-cell grading methods are based on direct optimization of the infill to obtain a porous, bone-like structure, under a local volume constraint. The compliance of these designs was slightly more than the compliance of unconstrained TO solutions, but were much more robust to changes in loading and material deficiency in the area where they were made, with redundant load paths still present. This robustness is useful when considering rotation; as well

as the explicit fatigue constraint in Eq. 9, the load cases introduced by imbalance, blade-loss and thermal transients are not enumerated and thus provided by local volume constraints [18].

IX. COMPARATIVE DISCUSSION AND CHALLENGES

A. Fatigue and Residual Stress Mitigation

The challenges for the fatigue resistance of additively manufactured parts reveal interwoven challenges, such as surface roughness, porosity and residual stress as well as the microstructure. Significant improvement in fatigue strength occurs with the machining and HIP and stress-relief treatments; however, the machining process cannot be used to access the inner raceways of the lattices, thus chemical finishing, HIP and design can have a significant influence. The reported fatigue strengths are less than one-half of the wrought values and if the lattice rotor was designed using the wrought allowables it would be a non-conservative design by two or more times [19]. The optimization strategies reviewed are compared in terms of design variables, fatigue treatment, thermal coupling, manufacturability and computation cost in table 6.

Table 6: Comparative Assessment of Lattice Optimization Strategies for Rotating Components

Approach	Design variable	Fatigue treatment	Thermal coupling	Manufactur-ability	Relative computational cost
Compliance-based SIMP	Element density	None	None	Requires interpretation and overhang filters	Low
Uniform lattice infill	Single relative density	Cell S–N data only	None	High	Very low
Graded lattice (homogenization)	Cell density field	Indirect, through stiffness	None	High, with connectivity control	Moderate
Infill with local volume constraint	Density with local volume bound	Implicit robustness	None	Moderate	Moderate to high
Stress-constrained TO	Element density	Static stress aggregation	Optional	Moderate	High
Thermo-fatigue-aware lattice	Cell density and orientation	Goodman with P-norm and defect knockdown	Build residual and service thermal	DfAM-filtered	High

Note. Qualitative scores derived from this comparison are visualized in Fig. 7.

The experimental measurement of residual stress confirms the necessity of the terms of the model based on thermal aspects. The tensile residual stresses measured by X-ray diffraction were found to be different for different scanning strategy/directions with respect to the scan

International Journal of Core Engineering & Management
Volume-6, Issue-12, 2021 ISSN No: 2348-9510

vectors (or x-y directions) for both the SLM 316L and Ti-6Al-4V samples, and were found to be greater for the Ti-6Al-4V [20]. Furthermore, surface residual stress is tensile without surface relief, and this surface residual stress is directly subtracted from the fatigue margin of Eq. 8, so it is recommended to consider the stress relief annealing process in the process chain; if the surface residual stress cannot be completely relieved, the measured data can be used as σres in Eq. 8.

B. Lattice Benchmarks and Unit-Cell Selection

Lightweight steel lattices are examples of mass savings that can be realized. The approach to scaling for design of these SLM-fabricated lattices is validated by power-law increases of the compressive moduli and yield strengths with increasing volume fraction for a set of unit-cell sizes of gyroid and diamond lattice structures of 316L stainless steel, which provides good geometric fidelity. The centrifugal load on a lattice region of a rotor at low volume fractions of lattices is small when compared with that of an equivalent solid region, and thus centrifugal load is also reduced.

The last factor that determines fatigue performance is the choice of unit-cell. It was found that for Ti-6Al-4V lattices both cell type and porosity affected S–N behavior and that differences in S–N behavior between the different topologies could be minimized by normalizing the stress by the yield stress of the material [22]. Based on the results and the comparison with Fig.7, here are some guidelines for designing a component that takes into account thermo-fatigue: Cells that are affected by a major stretching strain should be placed in high-stress areas near the bore.Cells affected by a major bending strain should be placed in areas with lower loads on the rim.Also, the fatigue allowables should be set after the design process, not based on the alloy itself.

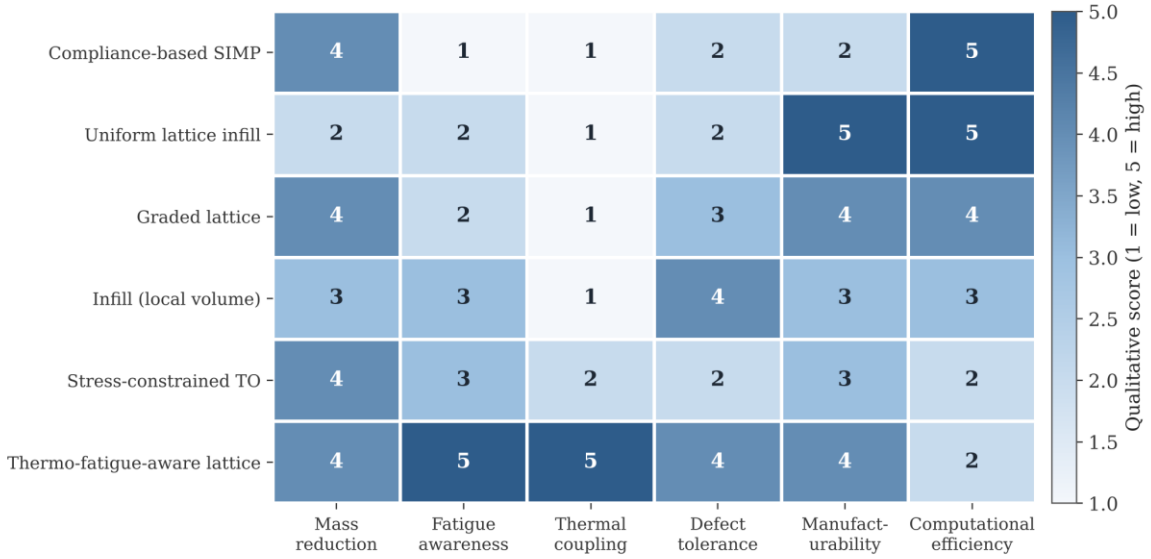


Figure 7: Qualitative Comparison of Lattice Optimization Strategies Across Six Design Criteria

X. CONCLUSION

This review brings together knowledge on processes, defects, fatigue, thermal effects, and optimization to create a design method for lattice structures in lightweight additively manufactured rotating parts.

The method focuses on minimizing mass while considering centrifugal and thermal balance, using a P-norm measure to combine a defect-adjusted Goodman criterion with manufacturing limits.Three main points come from this.First, fatigue allowables should be based on defect size, surface conditions, and the lattice design, not on data from wrought parts since the strength of as-built parts can be as low as half that of wrought parts, and the fatigue strength of lattices can be as low as 0.1 to 0.3 times the yield strength.Second, residual stress should be treated as mean stress, and stress relief should be required for rotors.Third, radial density grading: placing cells with the right density distribution to meet hoop stress needs, with stretching-dominated cells near the bore, can provide the best mix of mass reduction and durability.

More research is needed to create high-temperature fatigue data for superalloy lattices, to include real measured CT defect data directly in the design process, and to test full lattice rotors using spin-pit tests under combined thermal and centrifugal loads.

REFERENCES

1. N. T. Aboulkhair, N. M. Everitt, I. Ashcroft, and C. Tuck, “Reducing porosity in AlSi10Mg parts processed by selective laser melting,” Additive Manufacturing, vol. 1–4, pp. 77–86, 2014, doi: 10.1016/j.addma.2014.08.001.
2. M. M. Attallah, R. Jennings, X. Wang, and L. N. Carter, “Additive manufacturing of Ni-based superalloys: The outstanding issues,” MRS Bulletin, vol. 41, no. 10, pp. 758–764, 2016, doi: 10.1557/mrs.2016.211.
3. S. Beretta and S. Romano, “A comparison of fatigue strength sensitivity to defects for materials manufactured by AM or traditional processes,” International Journal of Fatigue, vol. 94, pp. 178–191, 2017, doi: 10.1016/j.ijfatigue.2016.06.020.
4. T. DebRoy, H. L. Wei, J. S. Zuback, T. Mukherjee, J. W. Elmer, J. O. Milewski, A. M. Beese, A. Wilson-Heid, A. De, and W. Zhang, “Additive manufacturing of metallic components – Process, structure and properties,” Progress in Materials Science, vol. 92, pp. 112–224, 2018, doi: 10.1016/j.pmatsci.2017.10.001.
5. G. Dong, Y. Tang, and Y. F. Zhao, “A survey of modeling of lattice structures fabricated by additive manufacturing,” Journal of Mechanical Design, vol. 139, no. 10, Art. no. 100906, 2017, doi: 10.1115/1.4037305.
6. A. du Plessis, I. Yadroitsava, and I. Yadroitsev, “Effects of defects on mechanical properties in metal additive manufacturing: A review focusing on X-ray tomography

insights," Materials & Design, vol. 187, Art. no. 108385, 2020, doi: 10.1016/j.matdes.2019.108385.
7. D. Herzog, V. Seyda, E. Wycisk, and C. Emmelmann, "Additive manufacturing of metals," Acta Materialia, vol. 117, pp. 371–392, 2016, doi: 10.1016/j.actamat.2016.07.019.
8. Y. Kok, X. P. Tan, P. Wang, M. L. S. Nai, N. H. Loh, E. Liu, and S. B. Tor, "Anisotropy and heterogeneity of microstructure and mechanical properties in metal additive manufacturing: A critical review," Materials & Design, vol. 139, pp. 565–586, 2018, doi: 10.1016/j.matdes.2017.11.021.
9. P. Li, D. H. Warner, A. Fatemi, and N. Phan, "Critical assessment of the fatigue performance of additively manufactured Ti–6Al–4V and perspective for future research," International Journal of Fatigue, vol. 85, pp. 130–143, 2016, doi: 10.1016/j.ijfatigue.2015.12.003.
10. K. Lietaert, A. Cutolo, D. Boey, and B. Van Hooreweder, "Fatigue life of additively manufactured Ti6Al4V scaffolds under tension-tension, tension-compression and compression-compression fatigue load," Scientific Reports, vol. 8, Art. no. 4957, 2018, doi: 10.1038/s41598-018-23414-2.
11. J. Liu, A. T. Gaynor, S. Chen, Z. Kang, K. Suresh, A. Takezawa, L. Li, J. Kato, J. Tang, C. C. L. Wang, L. Cheng, X. Liang, and A. C. To, "Current and future trends in topology optimization for additive manufacturing," Structural and Multidisciplinary Optimization, vol. 57, no. 6, pp. 2457–2483, 2018, doi: 10.1007/s00158-018-1994-3.
12. L. Liu, P. Kamm, F. García-Moreno, J. Banhart, and D. Pasini, "Elastic and failure response of imperfect three-dimensional metallic lattices: The role of geometric defects induced by selective laser melting," Journal of the Mechanics and Physics of Solids, vol. 107, pp. 160–184, 2017, doi: 10.1016/j.jmps.2017.07.003.
13. T. Maconachie, M. Leary, B. Lozanovski, X. Zhang, M. Qian, O. Faruque, and M. Brandt, "SLM lattice structures: Properties, performance, applications and challenges," Materials & Design, vol. 183, Art. no. 108137, 2019, doi: 10.1016/j.matdes.2019.108137.
14. T. Mukherjee, W. Zhang, and T. DebRoy, "An improved prediction of residual stresses and distortion in additive manufacturing," Computational Materials Science, vol. 126, pp. 360–372, 2017, doi: 10.1016/j.commatsci.2016.10.003.
15. O. Sigmund and K. Maute, "Topology optimization approaches," Structural and Multidisciplinary Optimization, vol. 48, no. 6, pp. 1031–1055, 2013, doi: 10.1007/s00158-013-0978-6.
16. M. K. Thompson, G. Moroni, T. Vaneker, G. Fadel, R. I. Campbell, I. Gibson, A. Bernard, J. Schulz, P. Graf, B. Ahuja, and F. Martina, "Design for additive manufacturing: Trends, opportunities, considerations, and constraints," CIRP Annals, vol. 65, no. 2, pp. 737–760, 2016, doi: 10.1016/j.cirp.2016.05.004.
17. Y. Wang, L. Zhang, S. Daynes, H. Zhang, S. Feih, and M. Y. Wang, "Design of graded lattice structure with optimized mesostructures for additive manufacturing," Materials & Design, vol. 142, pp. 114–123, 2018, doi: 10.1016/j.matdes.2018.01.011.
18. J. Wu, N. Aage, R. Westermann, and O. Sigmund, "Infill optimization for additive manufacturing—Approaching bone-like porous structures," IEEE Transactions on

Visualization and Computer Graphics, vol. 24, no. 2, pp. 1127–1140, 2018, doi: 10.1109/TVCG.2017.2655523.
19. A. Yadollahi and N. Shamsaei, "Additive manufacturing of fatigue resistant materials: Challenges and opportunities," International Journal of Fatigue, vol. 98, pp. 14–31, 2017, doi: 10.1016/j.ijfatigue.2017.01.001.
20. I. Yadroitsev and I. Yadroitsava, "Evaluation of residual stress in stainless steel 316L and Ti6Al4V samples produced by selective laser melting," Virtual and Physical Prototyping, vol. 10, no. 2, pp. 67–76, 2015, doi: 10.1080/17452759.2015.1026045.
21. C. Yan, L. Hao, A. Hussein, P. Young, and D. Raymont, "Advanced lightweight 316L stainless steel cellular lattice structures fabricated via selective laser melting," Materials & Design, vol. 55, pp. 533–541, 2014, doi: 10.1016/j.matdes.2013.10.027.
22. S. A. Yavari, R. Wauthle, J. van der Stok, A. C. Riemslag, M. Janssen, M. Mulier, J. P. Kruth, J. Schrooten, H. Weinans, and A. A. Zadpour, "Relationship between unit cell type and porosity and the fatigue behavior of selective laser melted meta-biomaterials," Journal of the Mechanical Behavior of Biomedical Materials, vol. 43, pp. 91–100, 2015, doi: 10.1016/j.jmbbm.2014.12.015.